

## X-ray determination of the electron density distribution in monoclinic $\text{Fe}_2(\text{SO}_4)_3$

P. C. Christidis, P. J. Rentzeperis

Applied Physics Laboratory, Aristotle University of Thessaloniki, Greece

A. Kirfel and G. Will

Mineralogisches Institut der Universität Bonn, Bonn, Federal Republic of Germany

Received: November 2, 1982

*Electron density / iron(III) sulfate / ferric sulfate*

**Abstract.** The electron-density distribution in monoclinic  $\text{Fe}_2(\text{SO}_4)_3$  at room temperature has been determined from precise single-crystal X-ray data. In order to study and reduce parameter bias, arising from bonding effects, separate least-squares refinements were performed on the high-order data ( $R = 0.039$ ) and the entire data set ( $R = 0.027$ ). Also a refinement based on a point charge model for the representation of positive residual charge accumulations was carried out ( $R = 0.019$ ). Difference density maps ( $X - X^{\text{HO}}$ ), based on the atomic parameters from the high-order refinement, were calculated in all interesting sections with special attention to the charge distribution within the  $[\text{SO}_4]^{2-}$  anions and around the Fe cations. Positive residual maxima of different heights, deviating in shape considerably from the rotational cylindrical symmetry of  $\sigma$ -bond charge accumulations, were observed on the S–O bond lines of the  $[\text{SO}_4]^{2-}$  anions, revealing strong polarization effects from the Fe cations. No residual electron density was observed on the Fe–O bond lines of the  $\text{FeO}_6$  octahedra, indicating that these bonds are primarily of ionic type. On the other hand significant density peaks were observed around the Fe cations in directions bisecting the Fe–O bond lines and at distances of about 0.4–0.5 Å from the atomic centers, revealing a deviation from the spherical distribution of the 3d electrons of the Fe ions.

### Introduction

Anhydrous iron(III),  $\text{Fe}_2(\text{SO}_4)_3$ , occurs in two crystalline forms, one monoclinic and one rhombohedral. Both yield well-formed transparent, light

pink crystals. The monoclinic crystals are of tabular or prismatic form, while the rhombohedral appear as isometric, cube-like rhombohedra in combination with triangular pinacoidal planes (001). The first X-ray study on  $\text{Fe}_2(\text{SO}_4)_3$  was performed by Kokkoros (1965), who observed the two crystal modifications of the compound and determined their crystallographic constants.

The room temperature crystal structure of the monoclinic iron(III) sulfate was determined independently by Moor and Araki (1974) (2414 reflections,  $R = 0.054$ ) and Christidis and Rentzeperis (1975) (4457 reflections,  $R = 0.038$ ). The structure can therefore be regarded as well established. It consists of an infinite three-dimensional network of corner-linked  $\text{SO}_4$  tetrahedra and  $\text{FeO}_6$  octahedra, so that each O atom is bonded to only one S and one Fe atom.

The magnetic properties of the compound have been studied extensively, especially during the past few years. A powder neutron diffraction study performed at 4.2 K (Long et al., 1979) showed that the nuclear structure of the monoclinic  $\text{Fe}_2(\text{SO}_4)_3$  remained essentially the same down to this temperature, while the magnetic structure indicated that it was a two-sublattice antiferromagnet. Magnetic susceptibility, Mössbauer and X-ray fluorescence studies performed at ambient and low temperatures indicated that the crystals are paramagnetic above 28.8 K with parameters typical for an octahedral high-spin iron(III) compound, and with a high degree of ionic character (Long et al. 1979, Haven and Nofle, 1977, Slater and Urch, 1972).

We have undertaken the determination of the electron density distribution in the monoclinic  $\text{Fe}_2(\text{SO}_4)_3$  in spite of its poor suitability factor (0.21) for such a study (Stevens and Coppens, 1976), and the relative complexity of its structure (153 standard atomic parameters) for the following reasons:

I. Although asphericities of the non-bonding 3d electrons around the octahedrally coordinated transition-metal atoms have been observed for a number of compounds, no charge distribution study has been performed so far for compounds with octahedrally coordinated Fe(III) ions.

II. A recent electron density distribution study on the mineral anhydrite,  $\text{CaSO}_4$ , (Kirfel and Will, 1980) indicated that the charge distribution within the  $[\text{SO}_4]^{2-}$  anion is considerably affected by the external bonding conditions, although earlier results on a number of sulfate compounds could lead to an opposite conclusion. It was thus considered of interest to perform a similar study of  $\text{Fe}_2(\text{SO}_4)_3$ , since even stronger polarization effects were expected for this compound.

It should be noted that the monoclinic iron(III) sulfate possesses some very suitable properties for such a study like good quality of crystals enabling the preparation of spheres for the X-ray experiment, very low temperature factors of the atoms and stable behaviour under radiation. These properties balance to some extent the drawbacks mentioned earlier, so that a meaningful

electron density distribution could be expected, provided that the intensity data were of very good quality.

### Experimental

Well formed single crystals of the monoclinic Fe<sub>2</sub>(SO<sub>4</sub>)<sub>3</sub> were prepared by the method described by Kokkoros (1965). The purity of the starting materials was of analytical grade. A number of well developed crystals was selected, placed into a special Nonius sphere grinder and shaped into spheres. Special precautions had to be taken, since the crystals are affected by the air moisture. The smallest spheres obtained were of about 0.3 mm in diameter. Attempts to prepare even smaller spheres failed. The crystal selected for the X-ray study was a sphere of 0.34 mm diameter with an uncertainty estimated to 4%. An analysis of intensity errors according to Vincent and Flack (1979), arising from the deviations of the selected sphere from ideal spherical shape, indicated that the application of a spherical absorption correction to the intensity data could be regarded as realistic. The crystal was sealed in a Lindemann capillary tube and centered on an automatic Philips PW 1100 four-circle, single crystal diffractometer. The unit cell dimensions were determined by least-squares methods from the angular setting of 59 independent reflections with  $2\theta > 58^\circ$ . The final values obtained are given in Table 1, together with results from earlier investigations for comparison. It is worth noting that the present results are identical, within their experimental errors, to those found in our earlier investigation (Christidis and Rentzeperis, 1975).

**Table 1.** Crystallographic data for monoclinic Fe<sub>2</sub>(SO<sub>4</sub>)<sub>3</sub>

	1	2	3	4
<i>a</i>	8.2973 (2) Å	8.2955 (12) Å	8.310 (2) Å	8.296 Å
<i>b</i>	8.5370 (2)	8.5332 (9)	8.558 (4)	8.515
<i>c</i>	11.6275 (3)	11.630 (2)	11.665 (4)	11.60
$\beta$	90.732 (2) <sup>o</sup>	90.75 (1) <sup>o</sup>	90.76 (3) (3) <sup>o</sup>	90.50
<i>V</i>	823.56 Å <sup>3</sup>	823.18 Å <sup>3</sup>	829.51 Å <sup>3</sup>	819.40 Å <sup>3</sup>

Space group: *P*2<sub>1</sub>/*n*

*Z* = 4

F.W. = 399.89

$\rho_{\text{meas}} = 3.20 \text{ Mg} \cdot \text{m}^{-3}$  (Kokkoros, 1965)

$\rho_{\text{calc}} = 3.225 \text{ Mg} \cdot \text{m}^{-3}$

$\mu(\text{MoK}\alpha) = 4.33 \text{ mm}^{-1}$

1 = This work

2 = Christidis and Rentzeperis (1975)

3 = Moor and Araki (1974)

4 = Kokkoros (1965)

Three-dimensional intensity data were collected on the PW 1100 diffractometer, using MoK $\alpha$  radiation, monochromated with a graphite monochromator. It was observed that low order reflections showed appreciable background asymmetry, when they were measured in the  $\theta/2\theta$  scan mode. Therefore, reflections with  $\theta < 25^\circ$  were measured in the  $\omega$ -scan mode and the rest of the reflections in the  $\theta/2\theta$  mode. Scan range and slit apertures were carefully selected in order to avoid any bias on the intensity measurements, due to the different scan modes used. Three standard reflections were monitored every 60 minutes. In addition, nine test reflections and their symmetry-equivalents (not related by center of symmetry) distributed throughout the reciprocal space were monitored at longer time intervals, as suggested by Abrahams (1974). The crystal was found to be very stable under radiation, since the variations of the check-intensities did not exceed  $\pm 1\%$  during the course of the measurement. All equivalent reflections were measured in the interval  $0 < \sin \theta/\lambda < 0.9 \text{ \AA}^{-1}$ , whereas only one hemisphere was scanned in the range  $0.9 < \sin \theta/\lambda < 1.11 \text{ \AA}^{-1}$ . Also, due to the very large number of reflections, only those with  $I_p - 2\sqrt{I_p} > I_b$ , where  $I_p$  and  $I_b$  are the peak and background intensities, were measured in this  $\sin \theta/\lambda$  interval. A total number of 29865 reflections was recorded. The integrated intensities were corrected for the usual geometrical factors and absorption, using the  $A^*$  values of Dwiggin (1975). The corrected intensities were then averaged, resulting in a set of 8768 unique reflections of which 1232 were regarded as unobserved ( $I < 2\sigma$ ). The internal agreement factor of the data, based on the deviations of the intensities of the equivalent reflections from their mean values was

$$R_{\text{int}} = \frac{\sum_{\mathbf{h}} \sum_i |F_{\mathbf{h},i}^2 - \bar{F}_{\mathbf{h}}^2|}{\sum_{\mathbf{h}} \sum_i F_{\mathbf{h},i}^2} = 0.033.$$

The variance assigned to each  $\bar{F}^2$  was computed by the equation

$$\sigma^2(\bar{F}^2) = \sigma_c^2(\bar{F}^2) + (0.033 \times \bar{F}^2)^2$$

where  $\sigma_c^2(\bar{F}^2)$  is the variance from the counting statistics alone.

### Structure refinements

The positional and thermal parameters from our earlier investigation (Christidis and Rentzeperis, 1975) were used as starting values for the conventional least-squares refinements. Atomic scattering factors and anomalous dispersion corrections for Fe, S and O were taken from the *International Tables for X-ray Crystallography* (1974). An isotropic extinction coefficient  $g$  (Zachariasen, 1967) was also included in the list of variables. The weighting scheme  $w = 1/\sigma^2(\bar{F}_o)$  proved to be the most satisfactory for our data. The following conventional least-squares refinements were carried out:

### I. All-data refinement

The full data set (8768 observations, 7536 contributing reflections) was used in this refinement. The main problem encountered at this stage was extinction, since for a number of reflections very large values of the extinction correction factor  $\kappa$  ( $\kappa^2 = \frac{I_{\text{corr}}}{I_{\text{obs}}}$ ) were obtained. The maximum value observed was 1.92 for the reflection 220, which corresponds to about 50 % reduction in its  $|F_o|$  value! However, the agreement obtained between the  $|F_o|$  and  $|F_c|$  values was very good, except for about twenty reflections with the largest  $\kappa$  values for which the extinction seemed to be slightly underestimated. In order to test whether the extinction model were realistic up to the largest extinction correction factors, all reflections with  $\kappa > 1.2$  were remeasured on a crystal with extremely small dimensions ( $25 \times 25 \times 50 \mu\text{m}$ ). To reduce its extinction effects further, the crystal was first cooled rapidly by dipping it into liquid air. The intensities of about 400 reflections (99 unique) were remeasured and converted in the usual way to the corresponding  $|F_o|$  values. Next, a refinement was carried out with only these reflections using fixed parameters from a high-order refinement (see below). Thus, only the scale factor and the extinction coefficient  $g$  were allowed to vary. The obtained  $R$  value was 0.031 ( $R_w = 0.039$ ). As expected, the  $g$  value for the second crystal was drastically reduced ( $g = 44 \times 10^{-7}$ ) in comparison with that of the first crystal ( $g = 683 \times 10^{-7}$ ). Accordingly the  $\kappa$  correction factor for the 220 reflection was 1.17 as compared to 1.92 found earlier. Assuming that the extinction model applied equally well to both crystals the ratio  $\kappa_{1,i}F_{1,i}/\kappa_{2,i}F_{2,i}$  should be constant. In this ratio  $\kappa_{1,i}$ ,  $\kappa_{2,i}$  represent extinction correction factors for the reflection  $i$  of crystals 1 and 2 and  $F_{1,i}$ ,  $F_{2,i}$  the corresponding observed structure amplitudes. Figure 1 shows the variation of this ratio versus the  $\kappa_1$  value to be essentially linear. In order to detect any systematic trend, a number of linear regression curves were computed by including more and more reflections with progressively larger  $\kappa$  values. The obtained results are given in Table 2. They show that the slopes of the regression curves are essentially zero, at least up to  $\kappa = 1.5$ , which means that the extinction corrections may be considered as realistic up to this value. The influence of the rest of the reflections on the atomic parameters is negligible, as it could be proved by a parallel refinement, omitting these reflections (about twenty). A  $\delta R$  normal probability plot (Abrahams and Keve, 1971), obtained at the end of the all-data refinement is presented in Figure 2. The great majority of the points lie approximately on a line with slope 1 passing through the origin, which indicates that the used weighting scheme can be considered acceptable. The final agreement factors obtained after convergence were  $R = 0.027$  ( $R_w = 0.038$ , goodness-of-fit GOF = 1.51). A list of the observed and calculated structure factors together with the atomic parameter tables from all refinements, which were performed in this study, have been deposited with the publisher of *Z. Kristallogr.*

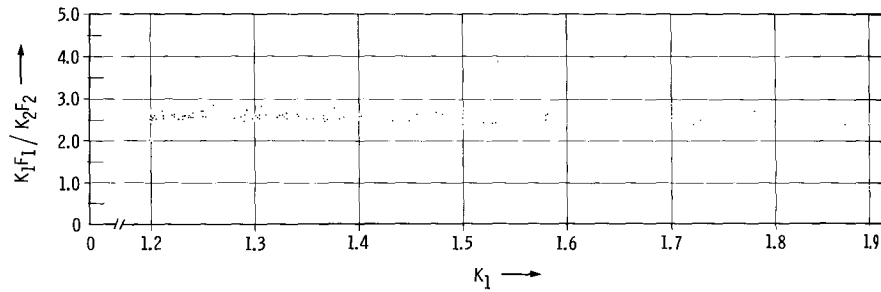


**Fig. 1.** Variation of the ratio  $\kappa_1 F_1 / \kappa_2 F_2$  versus  $\kappa_1$  for the reflections, which were severely affected by extinction. For the meaning of the symbols see text.  $F_1$  and  $F_2$  are in relative scales

**Table 2.** Regression coefficients for the points in Figure 1, determined for different cut-off values of  $\kappa$ . Equation of line:  $y = a_0 + a_1 x$

$\kappa$ cut-off values	$a_0$	$a_1$	Nr. of reflections
1.3	2.64 (24)	-0.06 (19)	44
1.4	2.62 (16)	-0.04 (12)	72
1.5	2.63 (12)	-0.05 (9)	84
1.6	2.75 (10)	-0.15 (8)	91
2.0	2.79 (7)	-0.17 (5)	99

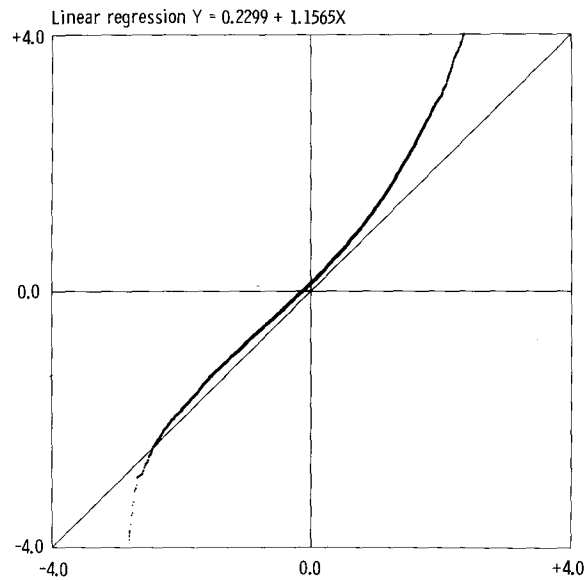


**Fig. 2.**  $\delta R$  normal probability plot, obtained at the end of the refinement Nr. 4 (all-data refinement). The horizontal axis represents expected ranked normal deviates and the vertical axis ordered experimental  $\delta R$ 's

**Table 3.** Results of the conventional refinements

	1	2	3	4	5
sin $\theta/\lambda$ ( $\text{\AA}^{-1}$ )	0–0.9	0.0–0.09	0.0–1.11	0.0–1.11	0.9–1.11
Nr. of observa- tions	5024	5024	8745	8768	3744
Nr. of con- tributing reflec- tions	4478	4478	7513	7536	3058
$R(\text{ov})$	0.025	0.024	0.038	0.037	0.059
$R(\text{omt})$	0.020	0.019	0.028	0.027	0.038
$R_w(\text{ov})$	0.032	0.028	0.051	0.040	0.041
$R_w(\text{omt})$	0.030	0.026	0.049	0.039	0.036
GOF	1.38	1.22	1.89	1.51	1.12
SC	1.1782 (13)	1.1686 (24)	1.1634 (14)	1.1667 (11)	1.1541 (65)
$g$	$721 (15) \times 10^{-7}$	$723 (15) \times 10^{-7}$	$696 (28) \times 10^{-7}$	$683 (15) \times 10^{-7}$	$677 \times 10^{-7}$

1 = Refinement with reflection up to sin  $\theta/\lambda = 0.9 \text{ \AA}^{-1}$

2 = Bond-model refinement

3 = All-data refinement without including extinction affected reflections

4 = All-data refinement with extinction affected reflections

5 = High-order refinement

## II. High-order refinement

In order to reduce possible bias on the atomic parameters due to bonding effects a high-order refinement was also carried out by using only reflections with  $\sin \theta/\lambda > 0.9 \text{ \AA}^{-1}$  (3744 observations, 3058 contributing reflections). The isotropic extinction coefficient  $g$  from the all-data refinement was also included but not varied. The agreement factors were  $R = 0.038$  ( $R_w = 0.036$ ) and  $\text{GOF} = 1.12$ . The atomic parameters derived from this refinement are presented in Table 4. Results from the Hirshfeld's  $z_{\text{A-B}}^2$  test on the physical significance of the thermal parameters in SO<sub>4</sub> groups (Hirshfeld, 1976) are given in Table 5. All r.m.s. discrepancies are of the order of one  $\sigma(U_{ij})$ , demonstrating the physical relevancy of the thermal parameters of the S and O atoms.

## III. Bond-model refinement

In a last refinement besides the standard atomic parameters also the parameters of point charges, placed on the midpoints of the interatomic bonds in the SO<sub>4</sub> tetrahedra, were varied (Kirfel and Will, 1980). The aim of this refinement was to check for a possible model improvement, and to test

**Table 4a.** Positional parameters ( $\times 10^5$ ) and equivalent isotropic temperature factors\* for monoclinic Fe<sub>2</sub>(SO<sub>4</sub>)<sub>3</sub>, obtained from the high-order refinement. E. s. d's are given in parentheses

	<i>x</i>	<i>y</i>	<i>z</i>	<i>B</i> <sub>eq</sub>
Fe(1)	74895(4)	46571(4)	61652(3)	0.47
Fe(2)	75302(4)	3484(4)	38427(3)	0.51
S(1)	3841(5)	25221(5)	49508(4)	0.47
S(2)	60409(4)	38136(5)	34909(3)	0.43
S(3)	60811(5)	11520(5)	64574(3)	0.47
O(1)	9004(18)	12687(18)	57349(13)	0.89
O(2)	-6014(19)	18910(20)	39969(12)	0.94
O(3)	18150(16)	32852(16)	44816(14)	0.86
O(4)	-5383(18)	36493(18)	56261(16)	0.99
O(5)	71252(20)	47917(21)	28059(12)	1.01
O(6)	43613(15)	41824(20)	31984(12)	0.86
O(7)	63550(20)	41117(21)	47100(11)	0.95
O(8)	62859(21)	21420(16)	32334(14)	0.95
O(9)	63273(20)	182(19)	73857(12)	0.94
O(10)	71179(25)	7211(27)	54931(15)	1.24
O(11)	43747(17)	11265(23)	61053(17)	1.09
O(12)	65311(21)	27239(16)	68560(12)	0.90

\* The equivalent isotropic temperature factor  $B_{eq}$  is defined by  $B_{eq} = 8 \pi^2 U_{eq}$ , where  $U_{eq} = \frac{1}{3} \sum_i \sum_j U_{ij} a_i^* a_j^* a_i \cdot a_j$ .

**Table 4b.** Anisotropic temperature coefficients ( $U_{ij} \times 10^5$ ) for monoclinic Fe<sub>2</sub>(SO<sub>4</sub>)<sub>3</sub>, obtained from the high-order refinement. E. s. d's are given in parentheses. Temperature factor:  $\exp \{-2 \pi^2 (U_{11} h^2 a^{*2} + U_{22} k^2 b^{*2} + U_{33} l^2 c^{*2} + 2 U_{12} h k a^* b^* + 2 U_{13} h l a^* c^* + 2 U_{23} k l b^* c^*)\}$ 

	<i>U</i> <sub>11</sub>	<i>U</i> <sub>22</sub>	<i>U</i> <sub>33</sub>	<i>U</i> <sub>12</sub>	<i>U</i> <sub>13</sub>	<i>U</i> <sub>23</sub>
Fe(1)	560(9)	586(9)	607(9)	-1(4)	14(4)	-53(4)
Fe(2)	626(9)	627(9)	652(9)	92(4)	7(4)	-30(4)
S(1)	503(10)	476(10)	727(7)	38(7)	70(6)	48(7)
S(2)	540(11)	578(11)	470(10)	58(7)	-7(6)	7(7)
S(3)	617(11)	642(11)	491(10)	-137(8)	-47(6)	38(7)
O(1)	1173(34)	972(34)	1259(36)	382(28)	43(27)	488(29)
O(2)	1160(35)	1338(39)	961(32)	-506(31)	-153(26)	10(29)
O(3)	799(29)	852(32)	1608(41)	-193(24)	369(27)	221(28)
O(4)	1027(34)	999(35)	1720(47)	370(28)	371(31)	-275(31)
O(5)	1287(38)	1602(46)	829(30)	-599(34)	171(26)	267(29)
O(6)	617(26)	1468(40)	1107(33)	429(26)	-154(23)	-278(29)
O(7)	1424(39)	1561(43)	509(25)	-54(33)	-162(24)	-134(26)
O(8)	1384(39)	689(29)	1450(40)	392(28)	-456(32)	-146(27)
O(9)	1530(42)	1092(35)	959(32)	-345(32)	-534(29)	451(29)
O(10)	1639(49)	1948(58)	997(35)	-20(43)	556(34)	-405(37)
O(11)	740(29)	1462(44)	1925(51)	-251(31)	-493(31)	519(40)
O(12)	1634(44)	748(30)	963(31)	-473(28)	142(29)	-79(24)

**Table 5.** Rigid-bond test for the thermal parameters of Table 4b. Mutual atomic vibrations  $z_{A,B}^2$  and  $z_{B,A}^2$  ( $\times 10^4 \text{ \AA}^2$ )

S(1)–O(1)	54	51	R.m.s. S(2)O <sub>4</sub>		3.50
S(1)–O(2)	72	74	S(3)–O(9)	54	54
S(1)–O(3)	50	49	S(3)–O(10)	65	64
S(1)–O(4)	53	56	S(3)–O(11)	58	56
			S(3)–O(12)	58	58
R.m.s. S(1)O <sub>4</sub>		2.40			
S(2)–O(5)	58	56	R.m.s. S(3)O <sub>4</sub>		1.12
S(2)–O(6)	51	46			
S(2)–O(7)	48	46			
S(2)–O(8)	56	60			

whether the residual charge accumulations observed in the ( $X - X^{\text{HO}}$ ) syntheses could be considered to describe bonding effects, reducing thus the bias of the standard atomic parameters. For practical reasons only reflections with  $\sin \theta / \lambda < 0.9 \text{ \AA}^{-1}$  were used (5024 observations, 4478 contributing reflections). No constraints were imposed on the multiplicities of the atoms and the point scatterers, but the positional parameters taken from the high-order refinement were kept fixed. In order to minimize correlation effects very low damping factors were used in the initial stage of the refinement and correlated variables were refined in subsequent cycles. The resulting agreement factors were  $R = 0.019$  ( $R_w = 0.026$ ) and  $\text{GOF} = 1.22$ . A parallel refinement ( $0 < s < 0.9 \text{ \AA}$ ) without the point scatterers was also carried out. The corresponding agreement factors were  $R = 0.020$  ( $R_w = 0.030$ ) and  $\text{GOF} = 1.38$ .

### Refinement results

A summary of the results of the different refinements is given in Table 4. The scale factors range between 1.1541 and 1.1782, corresponding to a model-dependent uncertainty of about 2%. The mean value 1.1634 was regarded as the most reliable estimate and therefore used in the ensuing calculations of the ( $X - X^{\text{HO}}$ ) syntheses. Correspondingly, the value  $g = 680 \times 10^{-7}$  was considered most appropriate for the extinction correction.

As mentioned earlier, the inclusion of reflections, which suffer most from extinction does not affect the derived parameters significantly. In fact, all the parameters from refinements (3) and (4) are identical at the  $1 \sigma$  level, where  $\sigma$  is the combined estimated standard deviation.

The comparison of the atomic parameters from all-data and high-order refinements shows that they generally agree at the  $1 \sigma$  level except in a few cases, where deviations up to  $3 \sigma$  are observed. In particular, a systematic

decrease is observed for the thermal parameters of the heavy atoms and to a lesser extent of the O atoms. Although a general decrease is almost always observed on going from the all-data to the high-order thermal parameters, the preferential decrease, observed for the heavy atoms in this study may be due to the inadequacy of the scattering factors owing to the uncertainty of the ionization state of the atoms. Since, however, the scattering factor curves of these atoms for different ionization states practically coincide in the  $\sin \theta/\lambda$  interval of the high-order refinement ( $0.9 - 1.11 \text{ \AA}^{-1}$ ), it is reasonable to expect a negligible bias on the high-order atomic parameters.

Finally, a comparison of the high-order positional parameters with those of our earlier study (Christidis and Rentzeperis, 1975) and those of Moor and Araki (1974) shows an agreement of all parameters at the  $1 \sigma$  level in the first case, whereas in the second case some significant deviations occur. In contrast to the very good agreement of the positional parameters, the deviations of the thermal parameters from those of both earlier studies are considerable.

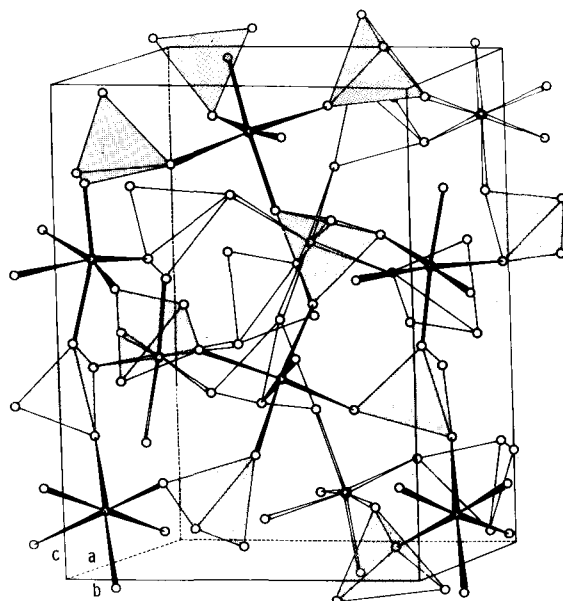
As far as the bond-model refinement is concerned, one can deduce from Table 3 that the improvement of the weighted R value is significant at the 0.005 significance level according to the Hamilton *R*-test (Hamilton, 1965). On the other hand, when the thermal parameters of refinements (1) and (2) are compared, one finds the bond-model parameters of the heavy atoms closer to the corresponding parameters from the high order-refinement, but the opposite is generally true for the O atoms. The net atomic charges, which were determined in this refinement by varying the atomic multiplicities do not seem to be reliable. All atoms appear neutral to within about  $1 \sigma$ , although there is evidence from other sources (e.g. Long et al., 1979) that the compound is ionic. A closer examination of this question is reserved for a future study. Distances and angles between the refined charge-cloud centers and the atoms are given in Table 6. Most of the point charges remained practically at their initial positions, e. g. half-way between the S and O atoms. However, the point charges E8, E12 and to a lesser extent E1, were drastically shifted towards the corresponding O atoms. This observation and the fact that for these point charges, as well as for E9, exceptionally high temperature factors were observed, explain well the general features observed on the corresponding ( $X - X^{\text{HO}}$ ) syntheses (see below).

### The crystal structure

Detailed descriptions of the structure of monoclinic iron(III) sulfate were given in earlier structural studies (Moor and Araki, 1974, Christidis and Rentzeperis, 1975). The structure consists of  $\text{SO}_4$  tetrahedra and  $\text{FeO}_6$  octahedra, connected through their corners. Each O atom is bonded to only one Fe and one S atom, forming an infinite three-dimensional network. A clinographic projection of the structure is shown in Figure 3. There are three

**Table 6.** Distances and angles for valence electron charge clouds from bond-model refinement

S(1)–E1	1.08(6) Å	O(1)–E1	0.48(6) Å	S(1)–E1–O(1)	138(8)°
S(1)–E2	0.87(3)	O(2)–E2	0.61(3)	S(1)–E2–O(2)	170(5)
S(1)–E3	0.76(3)	O(3)–E3	0.71(3)	S(1)–E3–O(3)	169(5)
S(1)–E4	0.75(4)	O(4)–E4	0.71(4)	S(1)–E4–O(4)	177(6)
S(2)–E5	0.68(4)	O(5)–E5	0.80(4)	S(2)–E5–O(5)	168(6)
S(2)–E6	0.91(4)	O(6)–E6	0.57(4)	S(2)–E6–O(4)	164(7)
S(2)–E7	0.77(4)	O(7)–E7	0.69(4)	S(2)–E7–O(7)	172(5)
S(2)–E8	1.40(2)	O(8)–E8	0.12(3)	S(2)–E8–O(8)	125(12)
S(3)–E9	0.84(5)	O(9)–E9	0.63(6)	S(3)–E9–O(9)	164(9)
S(3)–E10	0.75(3)	O(10)–E10	0.72(3)	S(3)–E10–O(10)	174(5)
S(3)–E11	0.71(3)	O(11)–E11	0.77(3)	S(3)–E11–O(11)	163(5)
S(3)–E12	1.40(3)	O(12)–E12	0.16(3)	S(3)–E12–O(12)	111(12)

**Fig. 3.** Clinographic projection of the structure of monoclinic  $\text{Fe}_2(\text{SO}_4)_3$ 

different  $\text{SO}_4$  tetrahedra and two  $\text{FeO}_6$  octahedra in the asymmetric unit. The  $\text{SO}_4$  tetrahedra are almost regular, having the same average S–O bond distance (1.467 Å) and bond angle (109.47°). The maximum deviations from these mean values are only 0.007 Å and 2.34° respectively. These values compare well with those from other sulfate compounds, e. g.  $\text{CaSO}_4$  (Kirkel and Will, 1980). The two  $\text{FeO}_6$  octahedra are only slightly distorted with mean bond distances of 1.981 and 1.995 Å and mean bond angles of 90.06° and 90.12° respectively. The maximum bond length deviations from the



mation maps were also computed by excluding from the Fourier summation those reflections (about twenty), which suffered most from extinction. We have found that the contribution of these reflections to the deformation maps was negligible, the significant peaks remained unaltered and only secondary features were changed. This can be understood, when we remember that the number of reflections contributing to the Fourier sums is very large (3236 unique reflections). Thus, in the ensuing calculations of deformation maps no reflections were omitted. The average standard deviation of the observed electron density at positions between atomic sites was estimated to be  $0.1 \text{ e}\text{\AA}^{-3}$  for a data cut-off value of  $\sin \theta/\lambda = 0.8 \text{ \AA}^{-1}$ . Since, however, this error becomes larger near crystallographic symmetry elements and especially at and near the atomic sites (Stevens and Coppens, 1976), in the present study only charge accumulations with heights greater than  $0.3 \text{ e}\text{\AA}^{-3}$  and at distances larger than  $0.3 \text{ \AA}$  from the atomic sites were considered significant.

#### *The $[\text{SO}_4]^{-2}$ tetrahedra*

Figure 5 represents deformation density maps in selected planes of the  $\text{SO}_4$  tetrahedra. The prominent features are the electron density accumulations on the S–O bonds, implying a covalent character of the bonding in the  $\text{SO}_4$  anion. The peak heights of most peaks are about  $0.6 \text{ e}\text{\AA}^{-3}$ , in agreement with results found in other sulfate compounds, e. g. sodium sulfanilate dihydrate (Bats, 1977), sodium dithionate (Kirfel and Will, 1980), or anhydrite (Kirfel and Will, 1980). On the other hand, the peak shapes clearly deviate from the rotational cylindrical  $\sigma$ -bond symmetry found for example in the first two mentioned sulfate compounds. Also deviations from the bond directions are observed for some peaks, as in the bonds S(1)–O(3) and S(2)–O(5). These findings are in agreement with those observed in anhydrite, supporting the conclusion that the electron density distribution within the  $\text{SO}_4$  anion can be considerably affected by the external bonding conditions. In contrast to anhydrite, however, vanishing density is observed on all bisectrices of the O–S–O angles. Also, another feature of the deformation maps not observed in the previously mentioned sulfate compounds, is that some peak heights are well below  $0.5 \text{ e}\text{\AA}^{-3}$ , e. g. in two extreme cases {bonds S(3)–O(9) and S(3)–O(12)} no peaks at all are observable. Considering the rigid bond test results and the bond distances there is nothing special about these bonds, which could imply that these findings are due to badly determined atomic parameters. A possible explanation of the observed inequality of the peak heights can be given, if one assumes aspherical distribution around the Fe atoms, which lead to preferential polarizations on the O atoms. In fact, we observe the “lone pair” electrons of these atoms to be extended towards Fe in a more pronounced way than in the case of the other atoms. The complete disappearance of the two mentioned peaks, however, is not clearly understood.

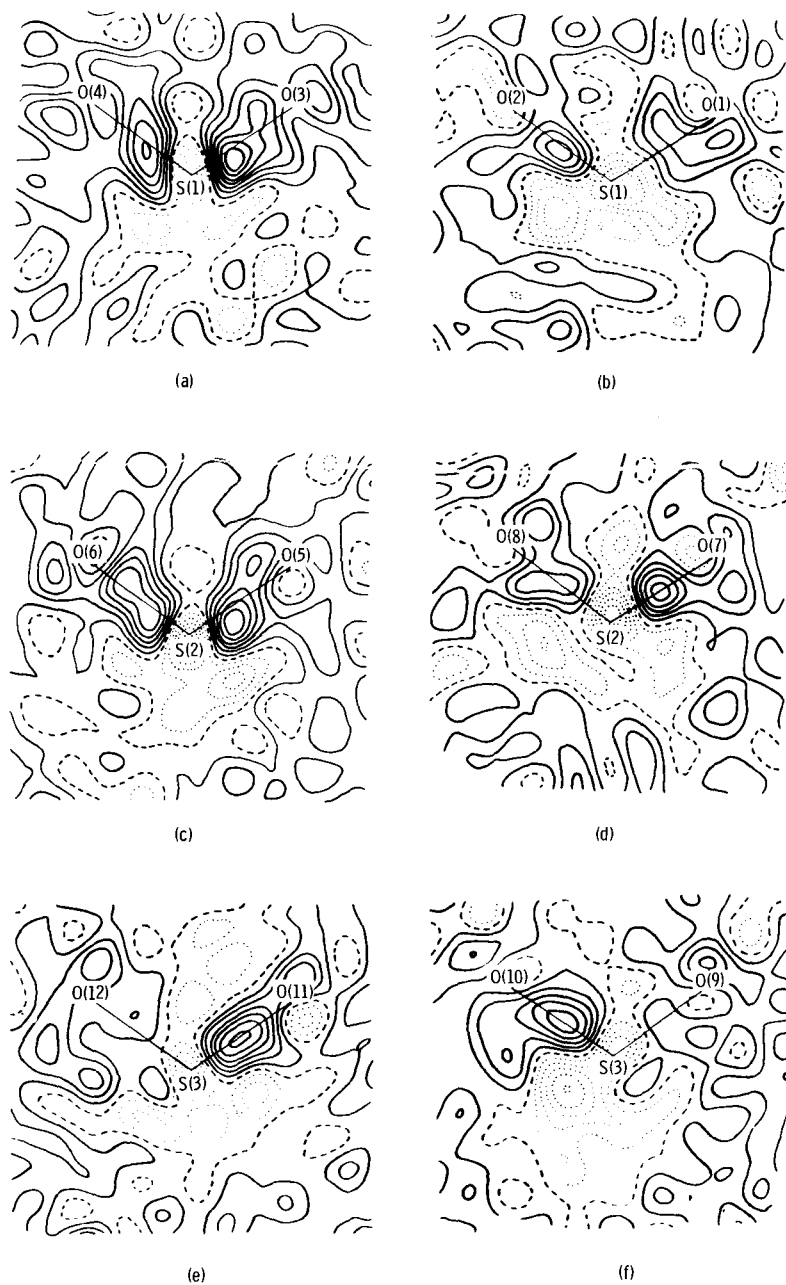


**Fig. 5.** Dynamic deformation density distribution in the  $[\text{SO}_4]^{2-}$  anions. Contours are at intervals of  $0.1 \text{ e}\text{\AA}^{-3}$ . Zero contours are broken, negatives are dotted. To identify sections see Figure 4

### The Fe sites

Figure 6 depicts selected density deformation sections in the two  $\text{FeO}_6$  octahedra. It should be noted, that both the  $\text{FeO}_6$  octahedra have the point group symmetry 1. Atoms shown to be connected by dashed lines lie out of plane, however, with maximum deviations not exceeding  $0.3 \text{ \AA}$ . The main characteristics of these sections are:

(I) No charge accumulations are observed on the Fe–O bond lines, thus indicating the prominent ionic character of the bonding in the  $\text{FeO}_6$  octahedra. This is in agreement with a quantitative estimation of the degree of covalency (Long et al., 1979) from Mössbauer data, which yielded about 6%.

(II) Significant charge accumulations with peak heights of about  $0.6 \text{ e\AA}^{-3}$  are observed around the Fe atoms, in directions bisecting the Fe–O lines. The distances from the associated nuclei are each about  $0.4 \text{ \AA}$ . This finding indicates a preferential population of the  $t_{2g}$  orbitals of the Fe atoms. There are, however, differences in the number of peaks and in the peak heights between the two crystallographically independent Fe atoms. Four peaks are observed around Fe(I) and six around Fe(2). In the first case, the number and arrangement of the peaks, as well as the peak heights, indicate a similarity to the deformation density observed around the Fe atom in fayalite,  $\alpha\text{-Fe}_2\text{SiO}_4$ , (Fujino et al., 1981). In the second case, the peaks are essentially directed towards the apices of a strongly distorted octahedron. The fact that significant charge accumulations are observed around the Fe atoms, suggests that the ionic state of these atoms should deviate from  $\text{Fe}^{3+}$ , since for this case a degenerate spherical configuration  $d^5$  is expected according to crystal field theory. The difference in the number of peaks, suggests additionally that the two Fe atoms are in different ionic states. These findings seem to be in disagreement with the results obtained from magnetic and Mössbauer measurements (Long et al., 1979), which indicate a  $d^5$  high-spin configuration for both Fe atoms. It should be noted, however, that a similar deviation from sphericity, has also been observed in tephroite,  $\alpha\text{-Mn}_2\text{SiO}_4$ , where the Mn atoms should exhibit a formal net charge 2+ and hence a spherical  $d^5$  electron configuration (Fujino et al., 1981).

### Conclusions

From the different refinements performed in the present study, it is deduced that the bias introduced from bonding effects in the derived atomic parameters is considerably less pronounced, than in analogous studies of molecular organic compounds. Since the determination of the electron density distribution in this study was based solely on X-ray data, this result is of particular importance.

The introduction of point charges to represent residual charge accumulations in the  $[\text{SO}_4]^{2-}$  anions (bond model refinement), resulted in a

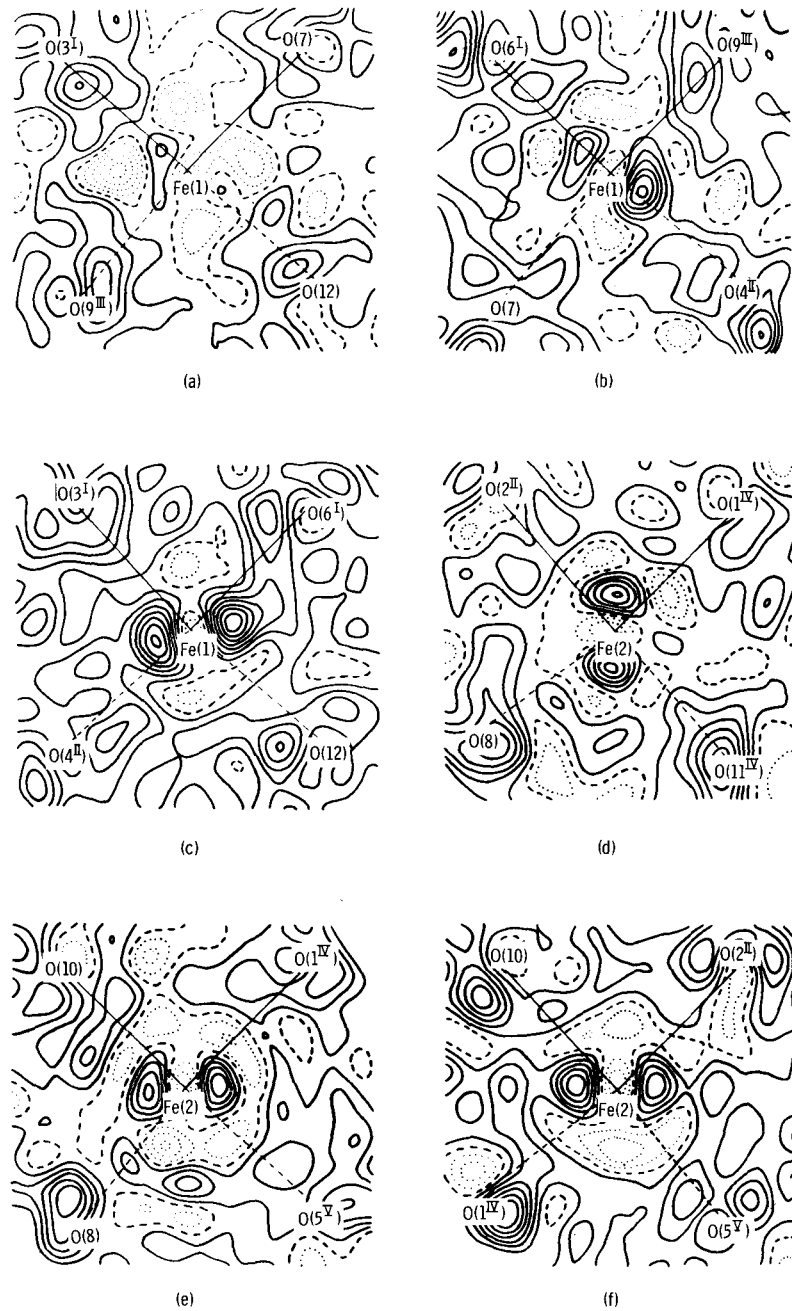


**Fig. 6.** Dynamic deformation density distribution in the  $\text{FeO}_6$  octahedra. Contours are as in Figure 5. To identify sections see also Figure 4

significant model improvement and led to the description, at least qualitatively, of the general features of the deformation density in these groups. However, the net atomic charges, derived from the refined atomic multiplicities are not in accordance with the values expected for ionic compound.

The observed deformation density revealed strong polarization effects from the Fe cations on the charge distribution within and around the  $[\text{SO}_4]^{2-}$  anions, supporting the conclusion from earlier investigations (Kirfel and Will, 1980), that the density distribution in these groups is considerably affected by external bonding conditions.

The absence of residual electron density on the Fe–O bond lines shows, that these bonds are mainly of ionic type. On the other hand, the density peaks observed around the Fe cations, can be considered as significant, indicating a deviation from the degenerate spherical distribution, expected for the  $\text{Fe}^{3+}$  ions in high-spin state.

*Acknowledgements.* Thanks are due to the Deutsche Forschungsgemeinschaft for support of this investigation. Also, one of the authors (P. C. C.) expresses his thanks to the Technical Assistance Service of the Greek Ministry of Coordination for a fellowship, that made his stay in West Germany possible.

## References

- Abrahams, S. C., Keve, E. T.: Normal probability plot analysis of error in measured and derived quantities and standard deviations. *Acta Crystallogr.* **A27**, 157–165 (1971)
- Abrahams, S. C.: The reliability of crystallographic structural information. *Acta Crystallogr.* **B30**, 261–268 (1974)
- Bats, J. W.: An electron density study of sodium sulfanilate dihydrate at 78 K. *Acta Crystallogr.* **B33**, 2035–2041 (1977)
- Christidis, P. C., Rentzeperis, P. J.: The crystal structure of the monoclinic  $\text{Fe}_2(\text{SO}_4)_3$ . *Z. Kristallogr.* **141**, 233–245 (1975)
- Dwiggins, C. W., Jr.: Rapid calculation of X-ray absorption correction factors for spheres to an accuracy of 0.05%. *Acta Crystallogr.* **A31**, 395–396 (1975)
- Fujino, K., Sasaki, S., Takeuchi, Y., Sadanaga, R.: X-ray determination of electron distributions in forsterite, fayalite and tephroite. *Acta Crystallogr.* **B37**, 513–518 (1981)
- Hamilton, W. C.: Significance tests on the crystallographic R factors. *Acta Crystallogr.* **18**, 502–510 (1965)
- Haven, Y., Nofle, R. E.: The Mössbauer isomer shift in iron(III) sulfate. *J. Chem. Phys.* **67**, 2825–2829 (1977)
- Hirshfeld, F. L.: Can X-ray data distinguish bonding effects from vibrational smearing? *Acta Crystallogr.* **A32**, 239–244 (1976)
- International Tables for X-ray Crystallography*, Vol. IV (1974) pp. 71–98 and 148–151. Birmingham: Kynoch Press
- Kirfel, A., Will, G.: Bonding in  $[\text{SO}_6]^{2-}$ : Refinement and pictorial representation from an X-ray diffraction study of  $\text{Na}_2\text{S}_2\text{O}_6 \cdot 2\text{H}_2\text{O}$  and  $\text{Na}_2\text{S}_2\text{O}_6 \cdot 2\text{D}_2\text{O}$ . *Acta Crystallogr.* **B36**, 512–523 (1980)
- Kirfel, A., Will, G.: Charge density in anhydrite,  $\text{CaSO}_4$ , from X-ray and neutron diffraction measurements. *Acta Crystallogr.* **B36**, 2881–2890 (1980)
- Kokkoros, P. A.: Röntgenuntersuchung der wasserfreien Sulfate der dreiwertigen Metalle Eisen, Chrom and Gallium. *Tschermaks MineralPetrogr. Mitt.* **10**, 45–51 (1965)

- Long, G. J., Longworth, G., Battle, P., Cheetham, A. K., Thundathil, R. V., Beveridge, D.: A study of anhydrous iron(III) sulfate by magnetic susceptibility, Mössbauer and neutron diffraction techniques. *Inorg. Chem.* **18**, 624–632 (1979)
- Moor, P. B., Araki, T.: Structural hierarchies among minerals containing octahedrally coordinating oxygen. III. The crystal structure of monoclinic ferric sulfate,  $\text{Fe}_2(\text{SO}_4)_3$ , and some intriguing topological questions. *Neues Jahrb. Mineral. Abh.* **121**, 208–228 (1974)
- Shannon, R. D., Prewitt, C. T.: Effective ionic radii in oxides and fluorides. *Acta Crystallogr.* **B25**, 925–946 (1969)
- Slater, R. A., Urch, D. S.: The origin of the  $K\beta'$  satellite peak in the X-ray fluorescence spectra of iron compounds: a correlation with magnetic susceptibility. *J. Chem. Soc. Chem. Commun.* 564–565 (1972)
- Stevens, E. D., Coppens, P.: A priori estimates of the errors in experimental electron densities. *Acta Crystallogr.* **A32**, 915–917 (1976)
- Vincent, M. G., Flack, H. D.: A priori estimates of errors in intensities for imperfectly spherical crystals. *Acta Crystallogr.* **A35**, 78–82 (1979)
- Zachariasen, W. H.: A general theory of X-ray diffraction in crystals. *Acta Crystallogr.* **23**, 558–564 (1967)